Electronic Supplementary Information

High Valence Transition Metals Doped Olivine Cathodes for Superior Energy and Fast Cycling Lithium Batteries

Gioele Pagot[1,2,*], Marco Bandiera[1,2], Keti Vezzù[1,2], Andrea Migliori[3], Renzo Bertoncello[4], Enrico Negro[1,2], Vittorio Morandi[3], and Vito Di Noto[1,2,*]

[1] Section of Chemistry for the Technology (ChemTech), Department of Industrial Engineering, University of Padova, Padova, Italy

[2] Centro Studi di Economia e Tecnica dell'Energia Giorgio Levi Cases, University of Padova, Padova, Italy

[3] National Research Council of Italy, Institute for Microelectronics and Microsystems – CNR IMM Section of Bologna, Bologna, Italy

[4] Department of Chemical Sciences, University of Padova, Padova, Italy

[*] To whom correspondence should be addressed. E-mail: vito.dinoto@unipd.it (V.D.N.), gioele.pagot@unipd.it (G.P.)

1. Reagents

Lithium metal, tantalum(V) oxide (>99.99%), polyvinyl difluoride (PVDF), 1-methyl-2-pyrrolidone (99.5%, anhydrous), lithium hexafluorophosphate (98%), ethylene carbonate (99%, anhydrous), and dimethyl carbonate (>99%, anhydrous) are purchased from Sigma-Aldrich. Lithium carbonate (99%) is obtained from BDH, ammonium phosphate dibasic (99%) from Riedel-de Haën, iron(III) oxide from Baker, nickel(II) oxide (97%), and cobalt(II) carbonate (50.5% assay) from Carlo Erba, niobium(V) oxide (>99.9%) from Fluka, graphite (SK6) from TIMCAL and carbon black (XC-72R) from Carbocrom. All materials are used as received.

2. Instruments Details

Stoichiometry is determined by using an inductively coupled plasma atomic emission spectrometer (ICP SPECTRO Arcos with EndOnPlasma torch), after digesting the samples with a hot mixture of HNO_3-HCl 1:3 (5 % in water solution); the emission lines are λ(Li) = 670.780 nm, λ(P) = 177.495 nm, λ(Fe) = 259.941 nm, λ(Ni) = 231.604 nm and λ(Co) =230.786 nm, λ(V) = 292.464 nm, λ(Nb) = 309.418 nm, λ(Ta) = 240.063 nm. The carbon content is determined with a Thermo Fisher FlashSmart elemental analyzer. Morphology and size distributions are studied by SEM microscopy using a Jeol JSM 5600 LV, equipped with an Oxford Instruments 6587 EDX detector, applying an accelerating voltage of 20 kV. After-cycling morphology studies are carried out by means of a FEI Inspect S50 SEM instrument using a 30 kV accelerating voltage. Microstructure is studied by a high-resolution transmission electron microscope TEM/STEM FEI TECNAI F20 at 200 keV mounting a high-angle collecting annular detector. XPS spectra are acquired using a Perkin Elmer Φ 5600ci spectrometer at a pressure < 10^{-8} mbar using a non-monochromatized Mg K_α excitation source ($h\nu$ = 1253.6 eV). The instrument is calibrated assigning a binding energy (BE) of 284.8 eV to the C_{1s} line of adventitious carbon. The structure of the materials is analyzed by powder wide-angle X-ray diffraction measurements using a GNR analytical

instrument (mod. eXplorer) with a Cu K_α source in the 2θ range 5-65 ° with a 0.02 ° step and integration time of 25 sec. Vibrational spectra (FT-MIR and FT-FIR) are obtained using a Nicolet Nexus spectrometer with a resolution of 2 cm^{-1}. FT-FIR measurements are collected in transmission by suspending the sample powder in anhydrous nujol and using polyethylene disks as windows. FT-MIR-ATR spectra are measured using a SPECAC Golden Gate single reflection diamond. The spectra are the result of an average of 1000 scans. For the electrochemical measurements, samples are manually ground with graphite (SK6) and PVDF. This mixture is suspended in 1-methyl-2-pyrrolidone producing an ink. For electrochemical impedance spectroscopy (EIS) and battery tests this ink is deposited and dried directly on a nickelated stainless steel current collector (loading is *ca*. 2.0 mg cm^{-2}). Cyclic voltammetry (CV) studies are conducted using a three-electrodes configuration. CV and EIS measurements are performed by using a Bio-Logic mod. VMP-300 instrument. Battery tests are carried out by a Maccor md. 2300. For CV tests the working electrode is a platinum wire covered by the cathodic material from the ink (*ca*. 1.6 mg cm^{-2}). Two lithium metal ribbons are used as the reference and the counter electrodes. The electrochemical tests are conducted at 25 °C using as an electrolyte a solution of 1 M $LiPF_6$ in EC/DMC 1:1 V/V. CV measurements are run from 3.5 to 5.0 V, at a scan rate of 5.0, 2.0, 1.0, and 0.5 mV s^{-1}. EIS spectroscopy measurements are carried out from 3 MHz to 40 mHz by using an EL-CELL and by fixing a ΔV of 4.600 V *vs*. Li/Li^+ with a potential oscillation of ±0.010 V. To allow the formation of a stable SEI, spectra are acquired on fully-charged cathodes after 10 charge/discharge cycles. Battery studies are performed by cycling a CR2032 coin cell between 3.5 and 5.0 V at different C rates (C=170 mA g^{-1}). The CR2032 is assembled using as anode a lithium metal foil of 13 mm of diameter. An initial conditioning of the cell is obtained by applying a cut-off in the charge process at the theoretical capacity value (170 mAh g^{-1}). For after-cycling morphology studies (300 cycles at 2C), the CR2032 battery is disassembled in a glove-box and the cathode electrode is thoroughly washed 5 times with DMC.

3. Structural refinements

Lattice parameters and atomic positions are obtained by Rietveld analysis. Refinement is performed by using as starting parameters those of the $LiCoPO_4$ structure (available in the Crystallography Open Database (COD), http://www.crystallography.net/, **COD ID** 2300246). The chemical composition of each phase is customized in accordance with ICP-AES results. Each structural parameter is optimized by minimizing the weighted R-factor profile, R_{wp}.

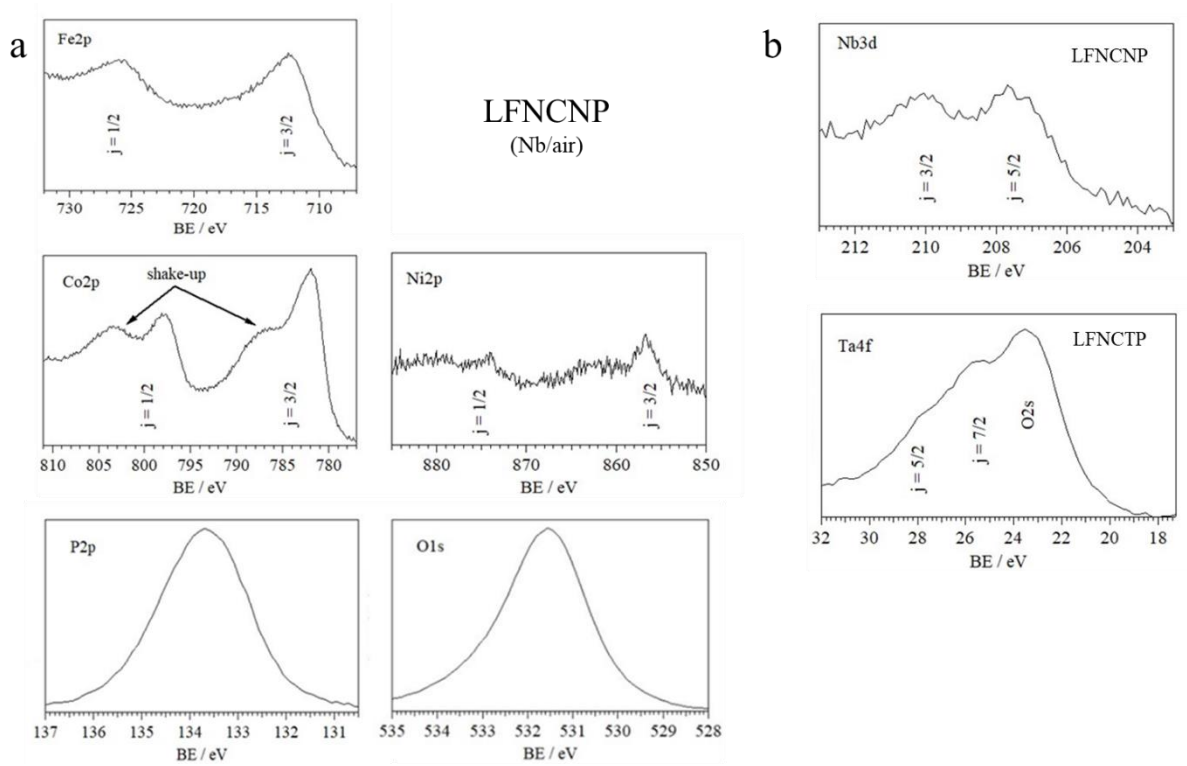

Figure S1. XPS analyses: Fe, Co, Ni, P, and O in LFNCNP sample (a); and Nb and Ta in the other samples (b).

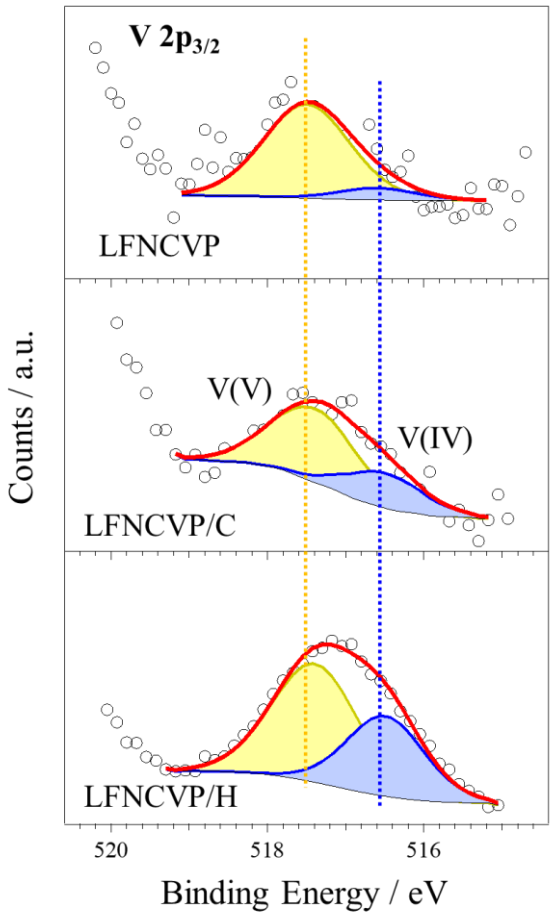

Figure S2. Decomposition of XPS $V_{2p_{3/2}}$ peak for samples of A group. The component attributed to V(V) and V(IV) is highlighted in yellow and blue, respectively.

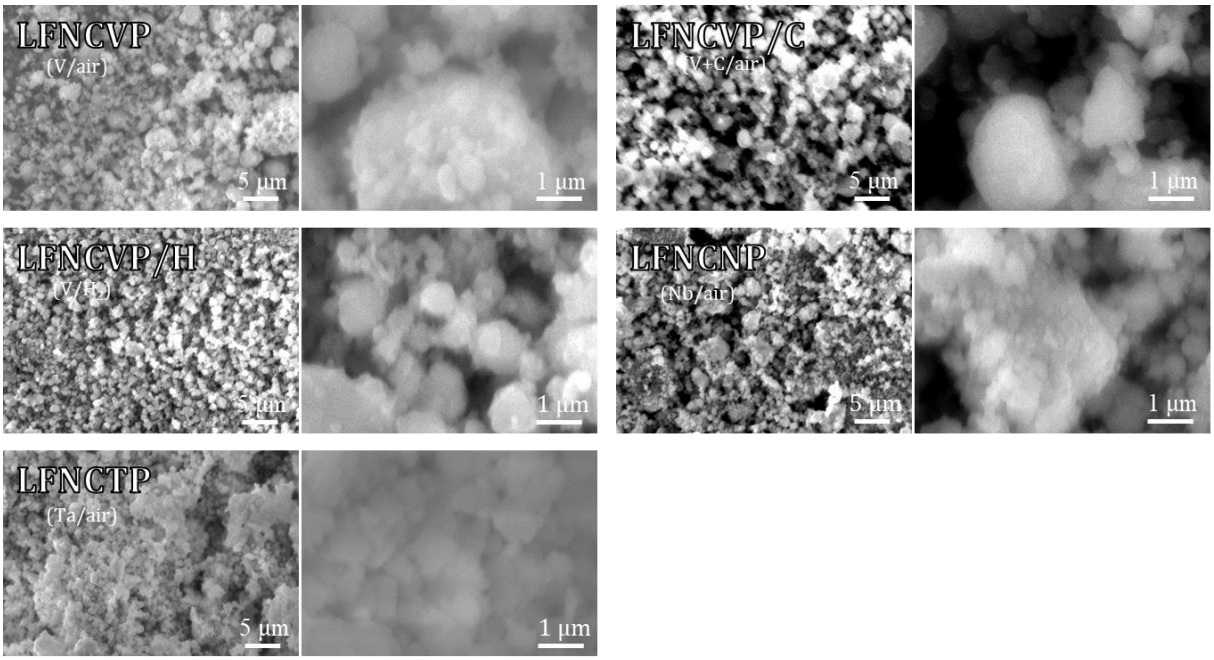

Figure S3. SEM images of samples obtained at different conditions (see Scheme 1).

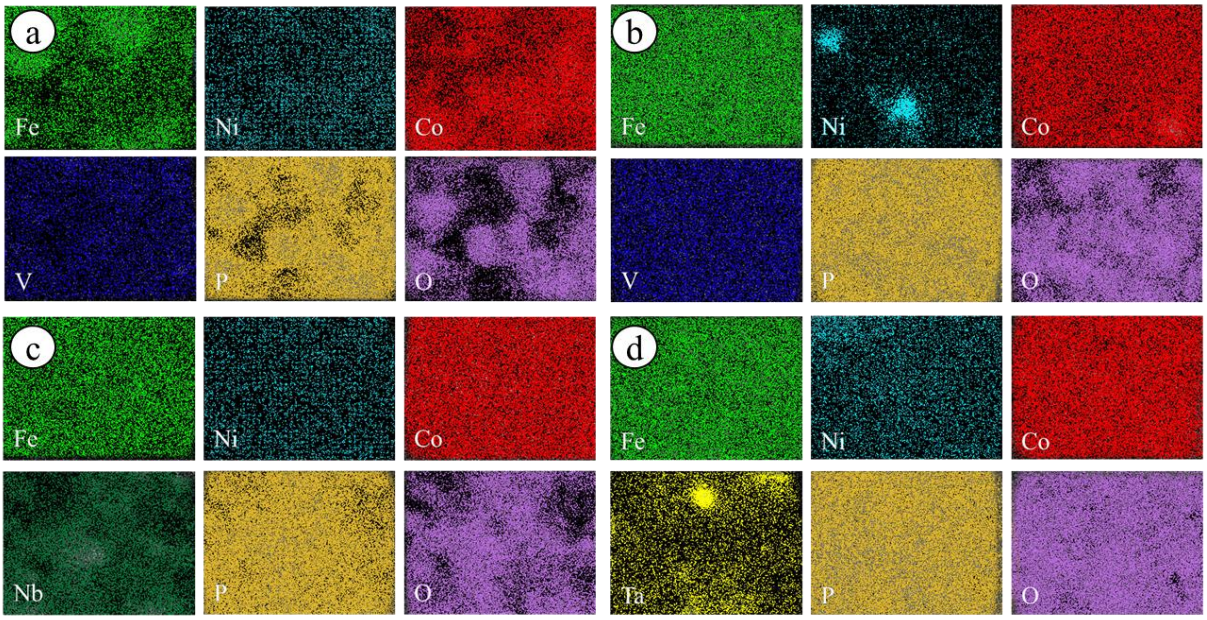

Figure S4. EDX: mapping of elements in LFNCVP/C (a), LFNCVP/H (b), LFNCNP (c), and LFNCTP (d).

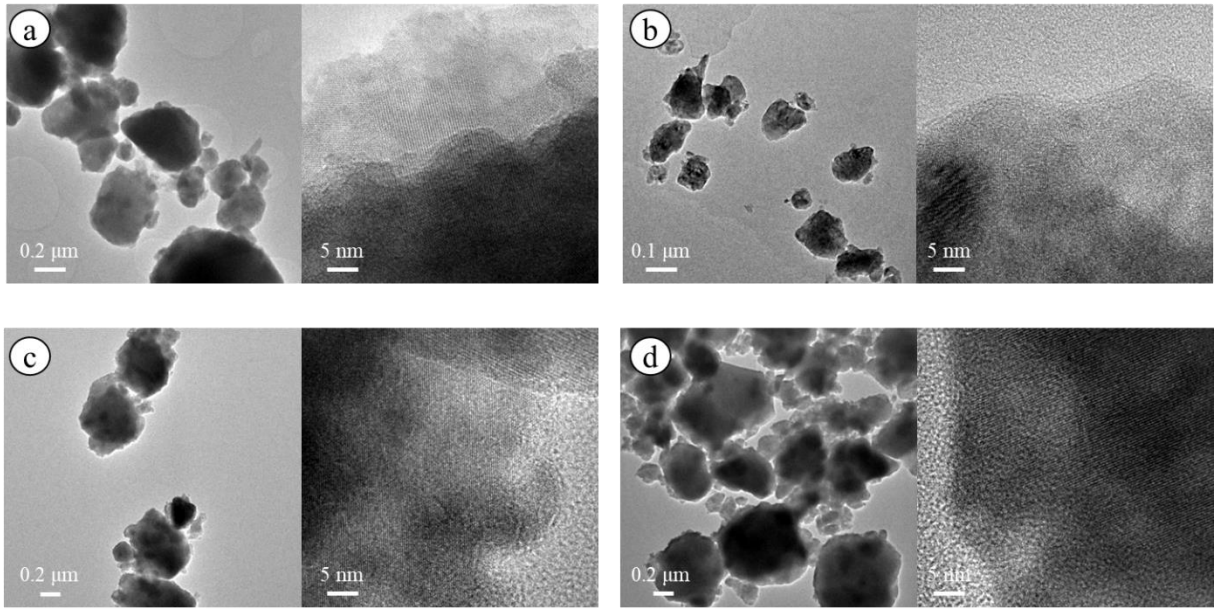

Figure S5. HR-TEM images of LFNCVP/C (a), LFNCVP/H (b), LFNCNP (c), and LFNCTP (d).

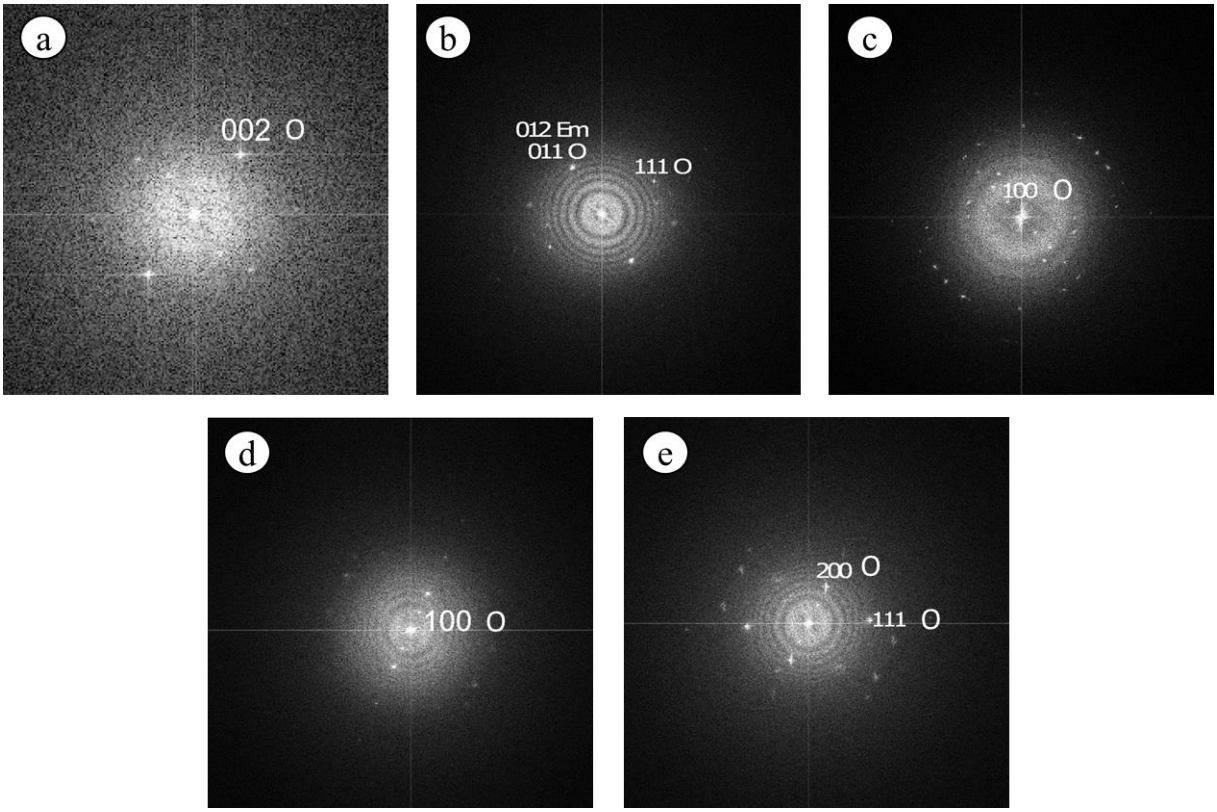

Figure S6. FFT of HR-TEM images of LFNCVP (a), LFNCVP/C (b), LFNCVP/H (c), LFNCNP (d), and LFNCTP (e). Miller indices are shown in the figure. O stands for Olivine, Em for hematite.

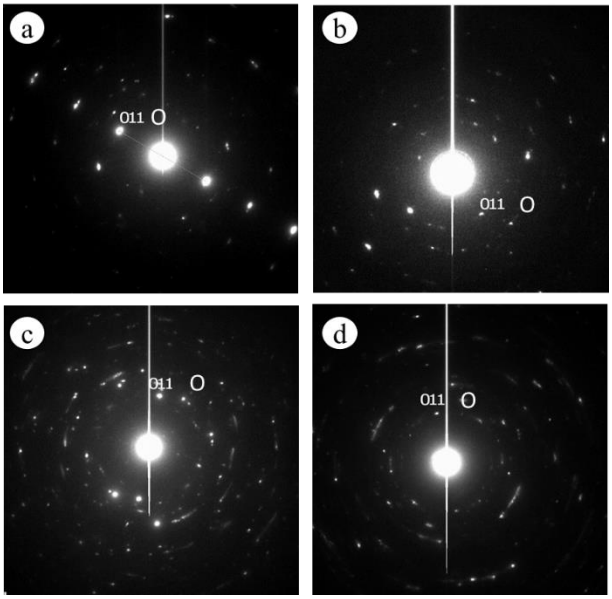

Figure S7. SAD images of LFNCVP/C (a), LFNCVP/H (b), LFNCNP (c), and LFNCTP (d). Miller indices are shown in the figure. O stands for Olivine.

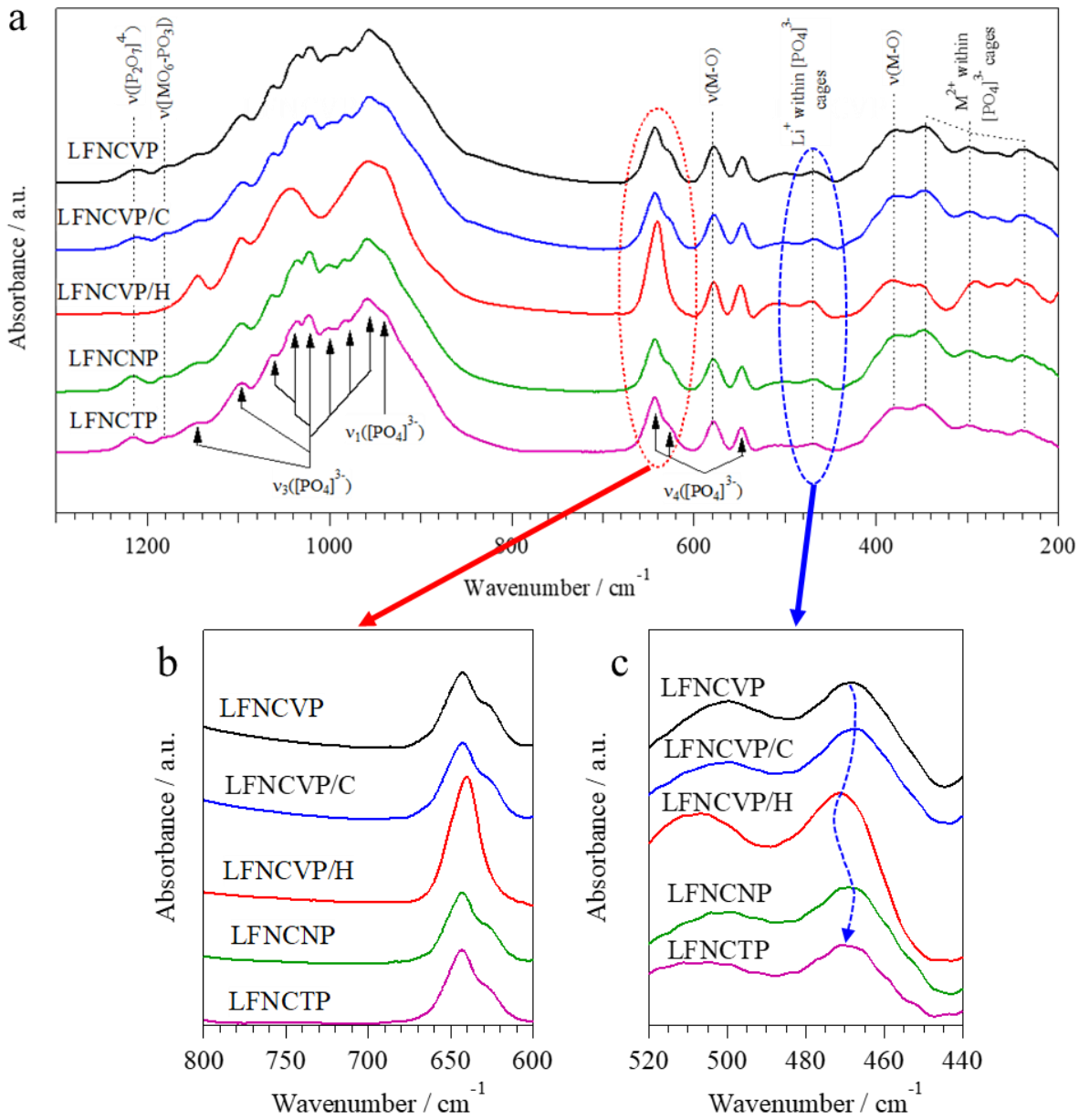

Figure S8. FT-MIR and FT-FIR spectra of synthetized samples with assigned vibrational modes (a). Spectral regions in the 600÷800 (b) and 440÷520 (c) cm^{-1} ranges.

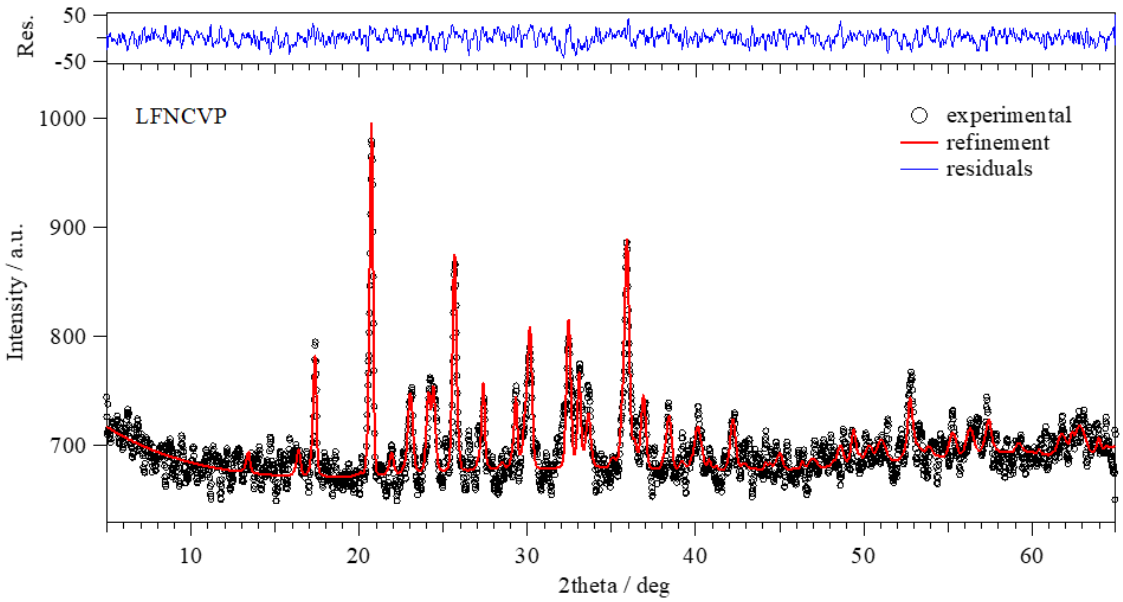

Figure S9. Rietveld analysis of LFNCVP sample (bottom panel). Residuals in the top panel.

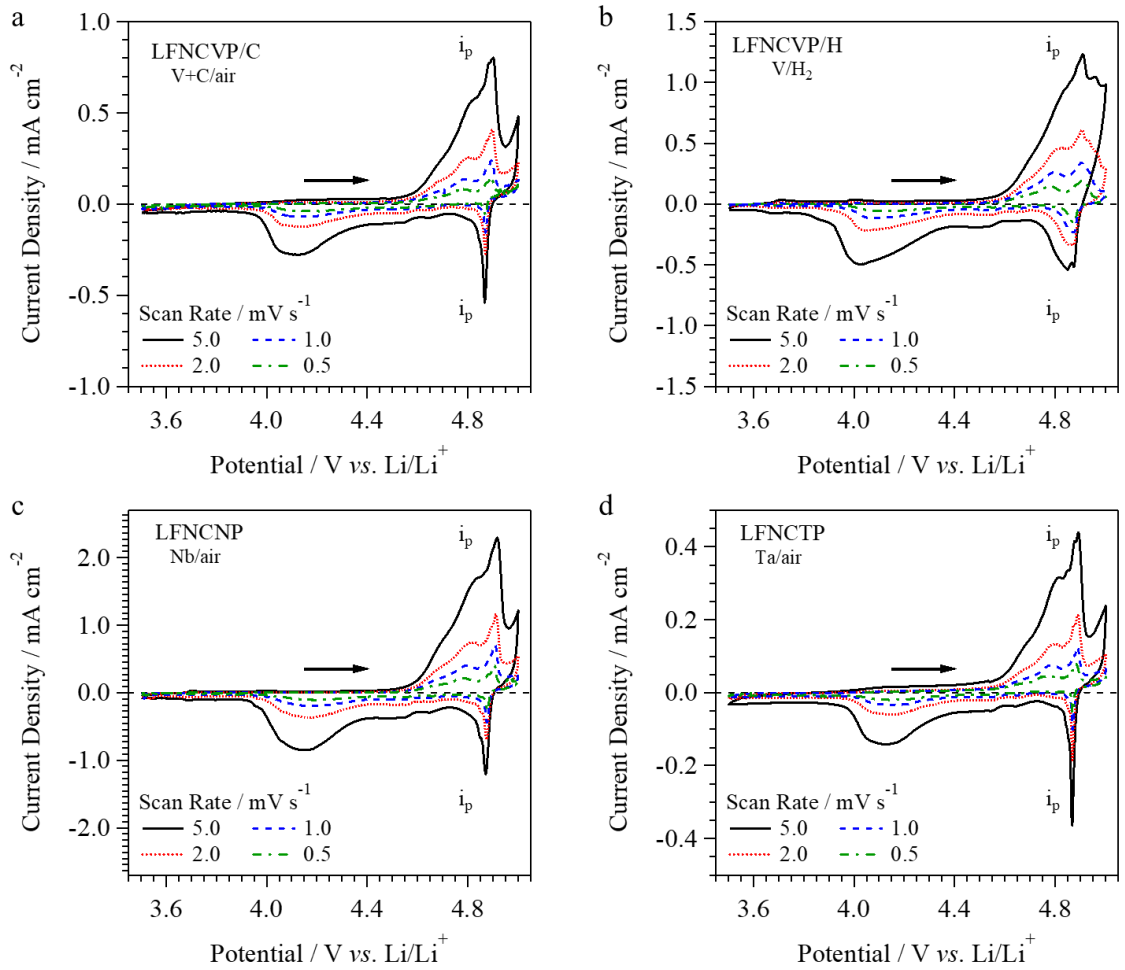

Figure S10. CV measurements of LFNCVP/C (a), LFNCVP/H (b), LFNCNP (c), and LFNCTP (d) at different scan rates. Cathodes are supported on a Pt wire. Two lithium metal ribbons are used as reference and counter electrodes, and 1 M $LiPF_6$ in EC/DMC 1:1 as electrolyte.

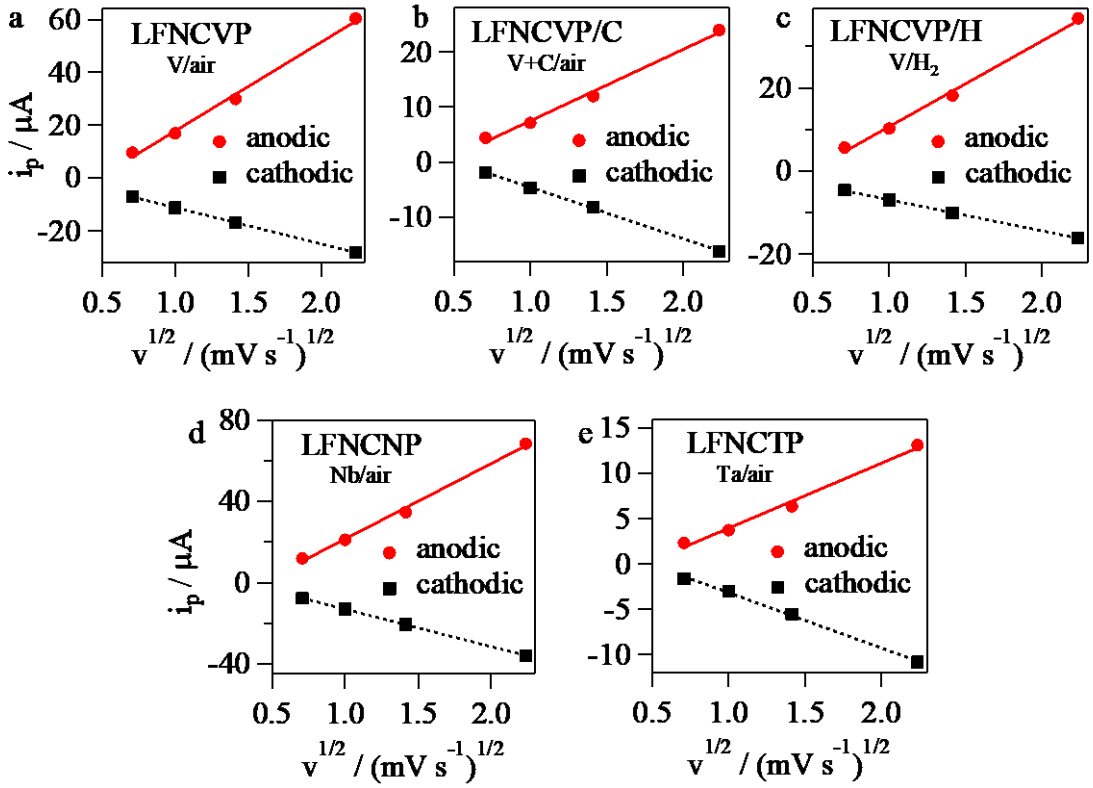

Figure S11. Current peak intensities, i_p (see Figure S9), *vs*. square root of the scan rate (v) for LFNCVP (a), LFNCVP/C (b), LFNCVP/H (c), LFNCNP (d), and LFNCTP (e). Data obtained from CV experiments.

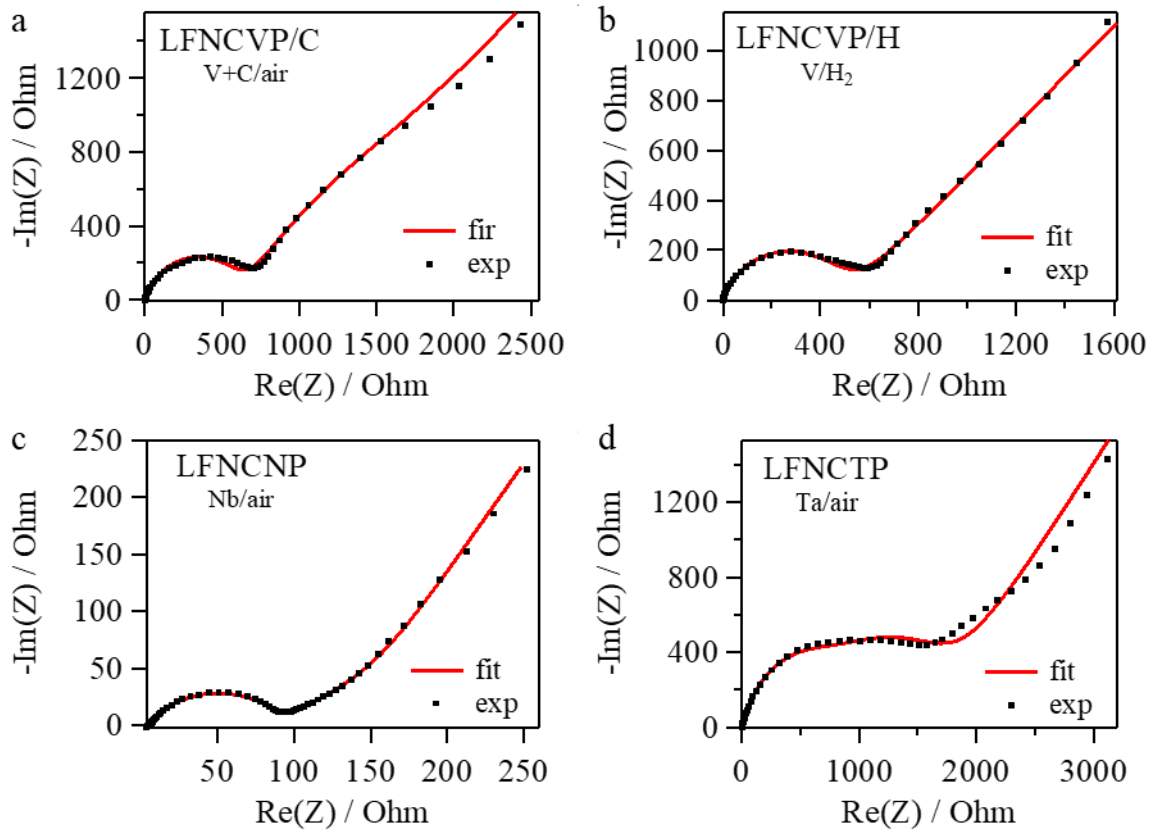

Figure S12. EIS spectra of LFNCVP/C (a), LFNCVP/H (b), LFNCNP (c), and LFNCTP (d).

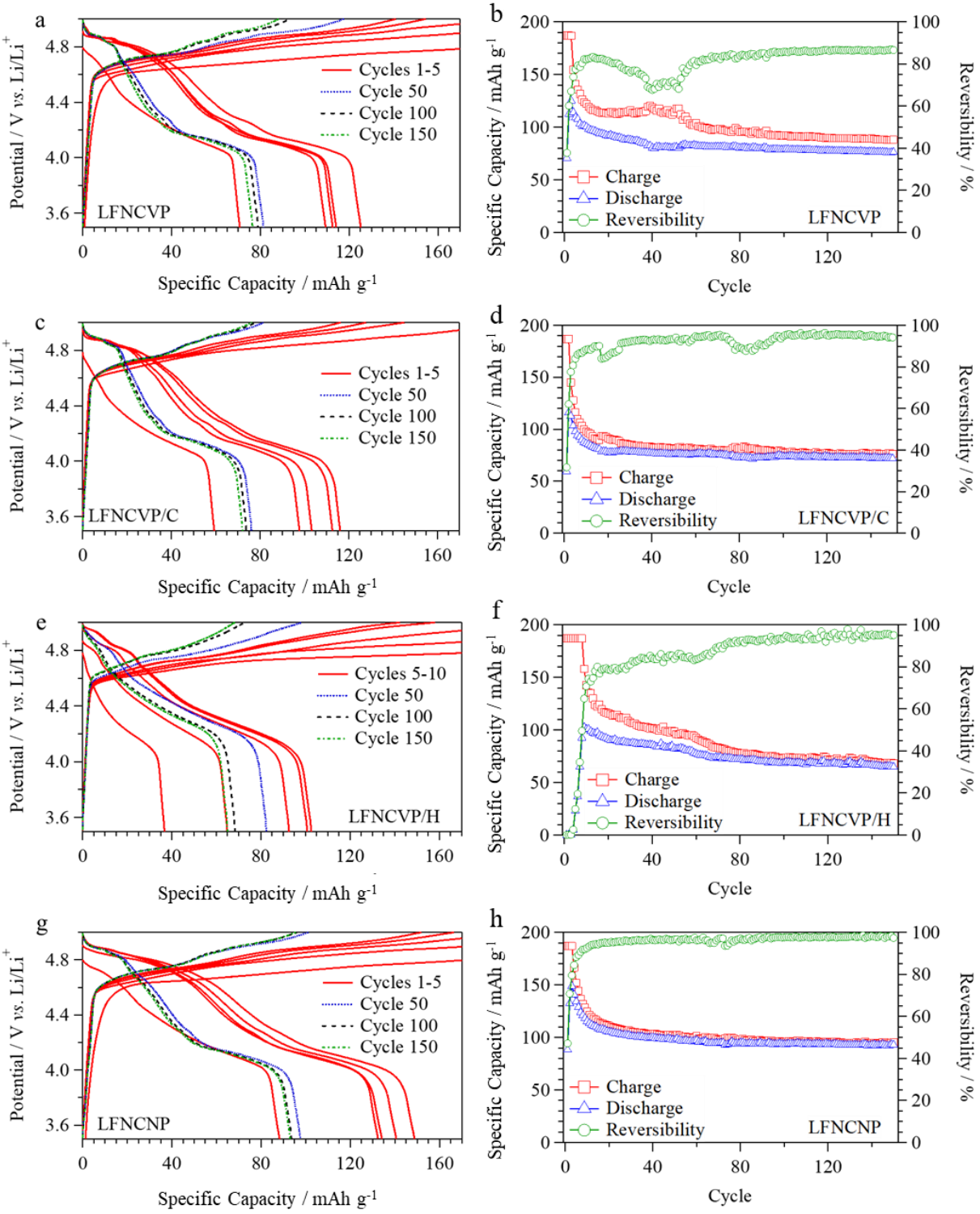
a
Potential / V vs. Li/Li+
Specific Capacity / mAh g-1
Cycles 1-5
Cycle 50
Cycle 100
Cycle 150
LFNCVP
b
Specific Capacity / mAh g-1
Reversibility / %
Cycle
Charge
Discharge
Reversibility
LFNCVP
c
LFNCVP/C
d
LFNCVP/C
e
Cycles 5-10
LFNCVP/H
f
LFNCVP/H
g
LFNCNP
h
LFNCNP

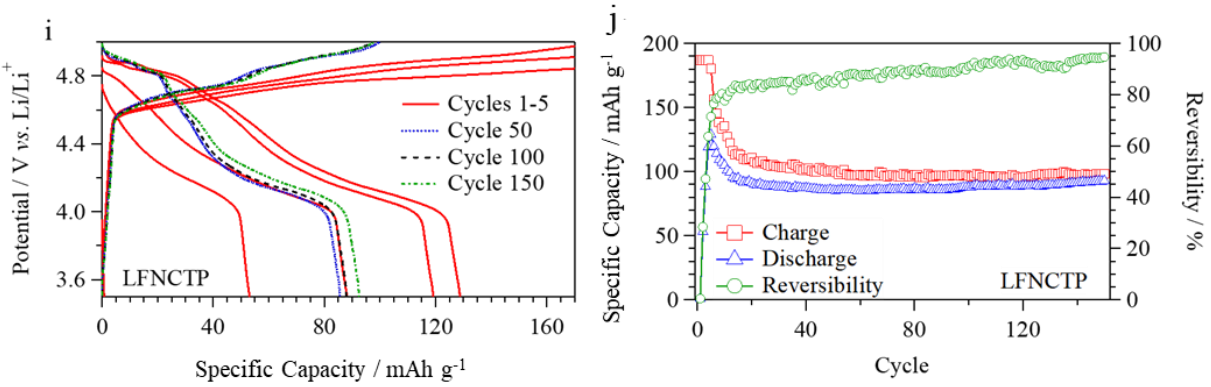

Figure S13. Galvanostatic battery tests on cycle numbers performed at C/5 for LFNCVP (a); LFNCVP/C (c); LFNCVP/H (e); LFNCNP (g); and LFNCTP (i). Durability tests in the first 150 cycles for LFNCVP (b); LFNCVP/C (d); LFNCVP/H (f); LFNCNP (h); and LFNCTP (j).

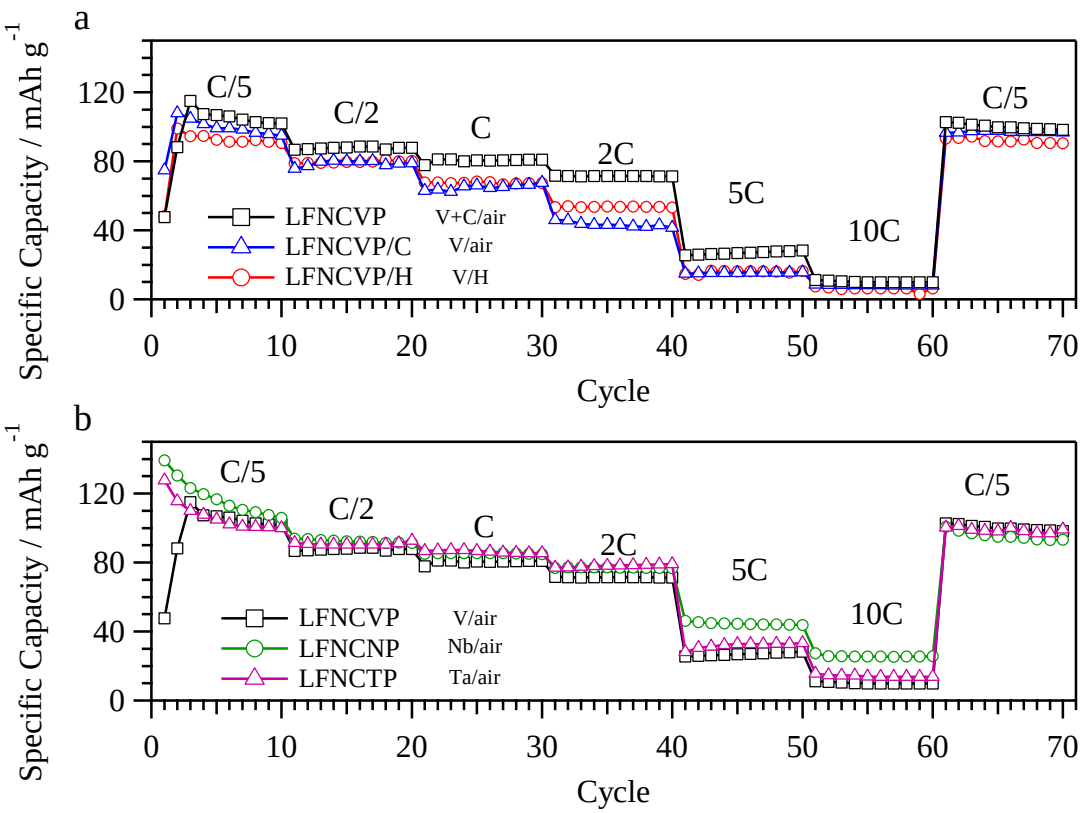

Figure S14. Dependence on cycle numbers of rate capability at different C for A (a) and B (b) groups. C = 170 mA g^{-1}.

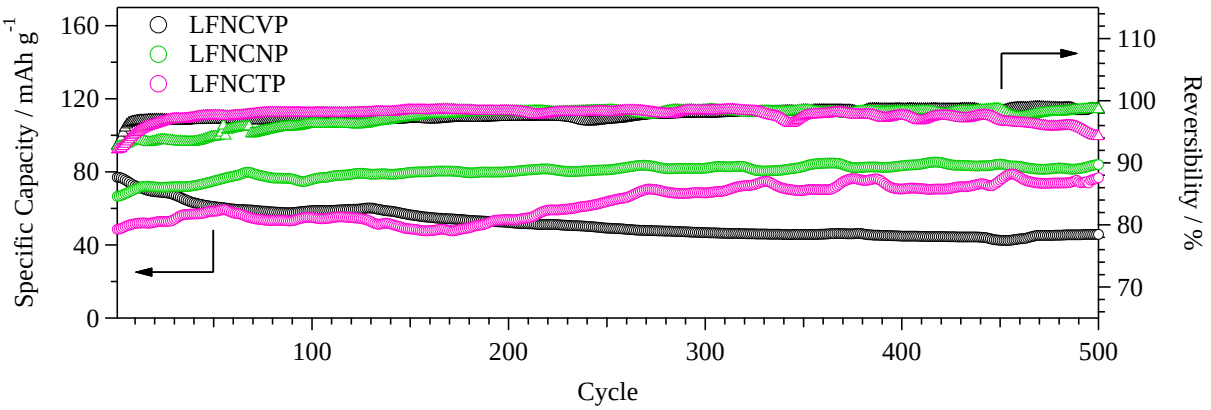

Figure S15. Long-term stability of LFNCVP, LFNCNP and LFNCTP samples cycled at 2C rate. Circles represent the specific capacity and triangles show the reversibility.

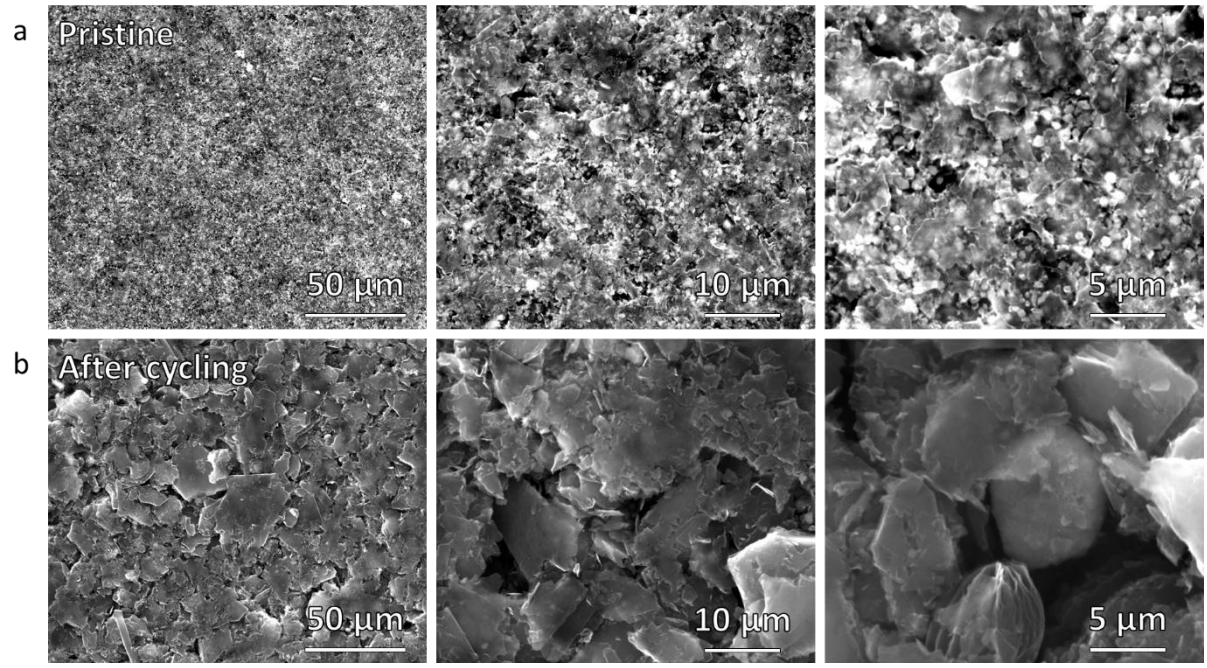

Figure S16. SEM images of pristine (a) and cycled (b) cathode electrode composed by LFNCNP material. The battery for after-cycling characterization is cycled for 300 cycles at 2C rate.

Table S1. Correlative assignments of FT-IR-ATR spectra of LFNCVP sample.

Wavenumber [a] / cm^{-1}	Assignment [b]	ref.
1212 (w)	$\nu([P_2O_7]^{4-})$	1, 2
1181 (w)	$\nu(MO_6\text{-}PO_3)$	2
1144 (w)	$\nu_3([PO_4]^{3-})$	3
1095 (s)	$\nu_3([PO_4]^{3-})$	3
1062 (s)	$\nu_3([PO_4]^{3-})$	3, 4
1035 (s)	$\nu_3([PO_4]^{3-})$	2
1022 (s)	$\nu_3([PO_4]^{3-})$	2, 4
997 (s,sh)	$\nu_3([PO_4]^{3-})$	4
982 (s)	$\nu_3([PO_4]^{3-})$	4
957 (s)	$\nu_3([PO_4]^{3-})$	3
940 (s,sh)	$\nu_1([PO_4]^{3-})$	2, 3, 5
643 (m)	$\nu_4([PO_4]^{3-})$	3
630 (m,sh)	$\nu_4([PO_4]^{3-})$	2
579 (m)	ν(M-O)	1, 5
547 (m)	$\nu_4([PO_4]^{3-})$	2, 3
469 (vw)	Li^+ within $[PO_4]^{3-}$ cages	3, 5
427 (vw,sh)	$\nu_2([PO_4]^{3-})$	2
378 (m)	ν(M-O)	5
347 (m)	M^{2+} within $[PO_4]^{3-}$ cages	3
299 (w)	M^{2+} within $[PO_4]^{3-}$ cages	3, 4
272 (vw)	rotation of $[PO_4]^{3-}$group+ M^{2+} transition	4
242 (w)	M^{2+} within $[PO_4]^{3-}$ cages	3, 4

[a] Relative intensities are reported in brackets; s: strong, m: medium, w: weak, vw: very weak, sh: shoulder. [b] ν_1 is the symmetric stretching of the phosphate group. ν_2 is the symmetric bending of the phosphate group. ν_3 is the antisymmetric stretching of the phosphate group. ν_4 is the antisymmetric bending of the phosphate group.

Table S2. Assignment of WAXD reflections of LFNCVP sample.

2theta / deg	*hkl* [a]	d_{hkl} [b] / Å	Phase	ref.
13.44	001	6.5836	$LiMP_2O_7$	[6]
16.37	020	5.4106	Li_3PO_4	[7]
17.40	200	5.0936	LMP	[8]
17.52	011	5.0593	$LiMP_2O_7$	[6]
20.76	101	4.2747	LMP	[8]
21.91	120	4.0535	Li_3PO_4	[7]
23.02	210	3.8597	LMP	[8]
23.04	-111	3.8575	$LiMP_2O_7$	[6]
23.18	101	3.8347	Li_3PO_4	[7]
24.14	011	3.6843	LMP	[8]
24.43	021	3.6403	Li_3PO_4	[7]
25.69	111	3.4647	LMP	[8]
25.74	201	3.4579	LMP	[8]
26.27	021	3.3892	$LiMP_2O_7$	[6]
27.38	101	3.2543	$LiMP_2O_7$	[6]
29.37	012	3.0389	$LiMP_2O_7$	[6]
29.91	211	2.9852	LMP	[8]
30.11	120	2.9653	$LiMP_2O_7$	[6]
30.19	020	2.9576	LMP	[8]
32.48	301	2.7544	LMP	[8]
33.07	104	2.7067	Fe_2O_3	[9]
33.62	220	2.6634	Li_3PO_4	[7]
35.57	110	2.5218	Fe_2O_3	[9]
35.94	311	2.4969	LMP	[8]
36.49	002	2.4602	Li_3PO_4	[7]
36.93	121	2.4322	LMP	[8]
38.45	410	2.3392	LMP	[8]
40.43	112	2.2291	$LiMP_2O_7$	[6]
42.22	112	2.1389	LMP	[8]
49.35	024	1.8451	Fe_2O_3	[9]
52.74	-104	1.7343	$LiMP_2O_7$	[6]
52.80	222	1.7323	LMP	[8]
52.91	402	1.7289	LMP	[8]

[a] Miller indices *hkl*. [b] Interplanar distances determined by Rietveld refinement.

Table S3. Quantification of the different crystalline phases composing the proposed cathode materials. Results are determined by means of the Rietveld refinement of WAXD curves.

Group	Sample	$LiMPO_4$	$LiMP_2O_7$	Fe_2O_3	Li_3PO_4	Ta_2O_5
A	LFNCVP	94.57±0.07	1.56±0.07	1.94±0.09	1.94±0.08	-
	LFNCVP/C	96.60±0.07	1.28±0.05	1.00±0.05	1.12±0.08	-
	LFNCVP/H	98.00±0.09	0.63±0.25	0.71±0.03	0.65±0.04	-
B	LFNCNP	93.82±0.06	2.20±0.13	1.85±0.07	2.12±0.07	-
	LFNCTP	92.03±0.07	2.12±0.29	2.29±0.14	1.94±0.22	1.61±0.05

Table S4. Lithium ion diffusion coefficients (D_{Li} / $cm^2\ s^{-1}$) of cathode materials at different scan rates. Values determined from CV experiments.

Group	Sample	Cathodic [a]				Anodic [b]			
		$D_{Li,5.0\ mV\ s^{-1}}$ / $cm^2\ s^{-1}$	$D_{Li,2.0\ mV\ s^{-1}}$ / $cm^2\ s^{-1}$	$D_{Li,1.0\ mV\ s^{-1}}$ / $cm^2\ s^{-1}$	$D_{Li,0.5\ mV\ s^{-1}}$ / $cm^2\ s^{-1}$	$D_{Li,5.0\ mV\ s^{-1}}$ / $cm^2\ s^{-1}$	$D_{Li,2.0\ mV\ s^{-1}}$ / $cm^2\ s^{-1}$	$D_{Li,1.0\ mV\ s^{-1}}$ / $cm^2\ s^{-1}$	$D_{Li,0.5\ mV\ s^{-1}}$ / $cm^2\ s^{-1}$
A	LFNCVP	$4.13\cdot10^{-12}$	$3.72\cdot10^{-12}$	$3.27\cdot10^{-12}$	$2.63\cdot10^{-12}$	$1.89\cdot10^{-11}$	$1.16\cdot10^{-11}$	$7.45\cdot10^{-12}$	$4.80\cdot10^{-12}$
	LFNCVP/C	$1.53\cdot10^{-12}$	$9.97\cdot10^{-13}$	$6.46\cdot10^{-13}$	$1.98\cdot10^{-13}$	$3.38\cdot10^{-12}$	$2.11\cdot10^{-12}$	$1.49\cdot10^{-12}$	$1.16\cdot10^{-12}$
	LFNCVP/H	$1.92\cdot10^{-12}$	$1.89\cdot10^{-12}$	$1.79\cdot10^{-12}$	$1.57\cdot10^{-12}$	$1.00\cdot10^{-11}$	$6.14\cdot10^{-12}$	$3.89\cdot10^{-12}$	$2.35\cdot10^{-12}$
B	LFNCNP	$7.98\cdot10^{-12}$	$6.62\cdot10^{-12}$	$5.33\cdot10^{-12}$	$3.73\cdot10^{-12}$	$2.90\cdot10^{-11}$	$1.86\cdot10^{-11}$	$1.38\cdot10^{-11}$	$8.90\cdot10^{-12}$
	LFNCTP	$1.83\cdot10^{-12}$	$1.19\cdot10^{-12}$	$7.08\cdot10^{-13}$	$4.06\cdot10^{-13}$	$2.68\cdot10^{-12}$	$1.58\cdot10^{-12}$	$1.09\cdot10^{-12}$	$8.47\cdot10^{-13}$

[a] Reduction process. [b] Oxidation process.

Table S5. Comparison between $D_{Li,EIS}$ and $D_{Li,CV}$. $D_{Li,EIS}$ and $D_{Li,CV}$ are the lithium diffusion coefficients evaluated from EIS and CV measurements, respectively.

Group	Sample	$D_{Li,CV}$ [a] / $cm^2\ s^{-1}$	Z_w / Ohm $s^{-1/2}$	$D_{Li,EIS}$ [b] / $cm^2\ s^{-1}$
A	LFNCVP	$3.44\cdot10^{-12}$	377.20	$1.97\cdot10^{-12}$
	LFNCVP/C	$8.44\cdot10^{-13}$	767.60	$8.68\cdot10^{-13}$
	LFNCVP/H	$1.80\cdot10^{-12}$	576.30	$1.92\cdot10^{-12}$
B	LFNCNP	$5.92\cdot10^{-12}$	248.20	$4.53\cdot10^{-12}$
	LFNCTP	$1.03\cdot10^{-12}$	787.20	$1.31\cdot10^{-12}$
R	LFNCP [c]	$5.61\cdot10^{-12}$	349.60	$4.58\cdot10^{-12}$

[a] CV measurements. [b] EIS experiments. [c] LFNCP is the reference cathode material (R).

Table S6. SEI resistance, charge transfer resistance and exchange current density values determined by EIS spectra.

Group	Sample	R_{SEI} / Ohm	R_{ct} / Ohm	i_0 [a] / mA cm^{-2}
A	LFNCVP	13.0	122.60	0.37
	LFNCVP/C	367.9	593.20	0.09
	LFNCVP/H	157.4	445.60	0.12
B	LFNCNP	12.6	87.50	0.52
	LFNCTP	759.2	857.30	0.06
R	LFNCP [b]	15.2	46.51	1.82

[a] Current density values are determined considering the geometrical area of the cathode materials. [b] LFNCP is the reference cathode material (R).

Supplementary References

1. A. A. Salah, P. Jozwiak, J. Garbarczyk, K. Benkhouja, K. Zaghib, F. Gendron and C. M. Julien, *J. Power Sources*, 2005, **140**, 370-375.

2. C. M. Julien, P. Jozwiak and J. Garbarczyk, Sofia, Bulgaria, 2004.

3. M. T. Paques-Ledent and P. Tarte, *Spectrochimica Acta Part A: Molecular and Biomolecular Spectroscopy*, 1974, **30**, 673-689.

4. W. Paraguassu, P. T. C. Freire, V. Lemos, S. M. Lala, L. A. Montoro and J. M. Rosolen, *Journal of Raman Spectroscopy*, 2005, **36**, 213-220.

5. C. M. Julien, A. Mauger, K. Zaghib, R. Veillette and H. Groult, *Ionics*, 2012, **18**, 625-633.

6. D. Riou, N. Nguyen, R. Benloucif and B. Raveau, *Mater. Res. Bull.*, 1990, **25**, 1363-1369.

7. R. W. G. Wyckoff, *The Structure of Crystals: Supplement for 1930-1934 to the Second Edition*, Reinhold Publishing Corporation, Hoboken, NJ, USA, 1935.

8. T. Kimura, C. K. Chang, F. Kimura and M. Maeyama, *J. Appl. Crystallogr.*, 2009, **42**, 535-537.

9. L. Pauling and S. B. Hendricks, *J. Am. Chem. Soc.*, 1925, **47**, 781-790.